STRUCTURE OF THE SUBDUCTION SYSTEM IN SOUTHERN PERU FROM SEISMIC ARRAY DATA

Kristin Phillips[1], Robert W Clayton[1], Paul Davis[2], Hernando Tavera[3], Richard Guy[2], Steven Skinner[1], Igor Stubailo[2], Laurence Audin[4], Victor Aguilar[3]

[1]Caltech Seismological Laboratory, Pasadena CA, United States, [2]UCLA Center for Embedded Networked Sensing, UCLA, Los Angeles, CA, United States, [3]Instituto Geofisico del Peru, Lima, Lima 100, Peru, [4]IRD, Casilla 18-1209, Lima 18, Peru

Abstract

The subduction zone in southern Peru is imaged using converted phases from teleseismic P, PP, and PKP waves. The receivers are a linear array of 50 broadband seismic stations spanning 300 km from Mollendo on the coast to Juliaca near Lake Titicaca. The slab dips at 30 degrees and can be observed to a depth of over 200 km. The Moho is seen as a continuous interface along the profile and the crustal thickness in the back-arc region (the Altiplano) is 75 km thick which is sufficient to isostatically support the Andes. At the mid-crustal level of 40 km, there is a continuous structure with a positive impedance contrast, which we suggest is the western extent of the Brazilian Craton as it under-thrusts to the west. Vp/Vs ratios estimated from receiver function stacks show an average value of about 1.75 for this region. The results support a model of crustal thickening in which the margin crust is under-thrust by the Brazilian shield rather than delamination of lower crust through eclogitization.

Introduction

The subduction of the Nazca plate in southern Peru represents a transition region from a shallow-dip system in northern and central Peru to normal-dip in southern Peru. The flattening of the slab in northern and central Peru has been proposed to be due to factors such as the subduction of anomalous crustal features such as the Nazca Ridge (Gutscher et al., 2000) which has been sweeping southward over time due to its oblique subduction angle (Hampel, 2002). The slab has been progressively flattening in the wake of this feature, and its present configuration is shown in Figure 1 which also shows slab contours and the location of the volcanic arc. In this paper, we focus on the region of normal-dip subduction south of Nazca Ridge that we assume represents the subduction system before the flattening process. This system is analyzed using data from a linear array of 50 stations (shown in Figure 1) deployed perpendicular to the subduction trench for a distance of 300 km, with an average interstation spacing of 6 km. The slab dip can be imaged from seismicity and results from this study have confirmed that the slab dips at about 30 degrees along the array. A positive impedance mid-crustal structure observed at about 40 km depth is proposed to be a result of underthrusting of the Brazilian Shield (McQuarrie et al., 2005; Allmendinger et al, 1996; Horton et al., 2001; Gubbels et al., 1993; Lamb & Hoke, 1997; Beck & Zandt, 2002), which is more consistent with a gradual uplift model of the Altiplano which suggests a continuous rise over the last 40 Ma (Barnes and Ehlers, 2009; Ehlers and Poulsen, 2009; McQuarrie et al., 2005; Elger et al., 2005; Oncken et al., 2006). In contrast others have proposed that lithospheric delamination resulted in the rapid rise of the Andes in the last 10 Ma (Gregory-Wodzicki, 2000; Garzione et al, 2006, 2008; Ghosh et al., 2006). We present a detailed image of the slab and lithosphere based on receiver functions and tomography that establishes the basic structure and properties of this region.

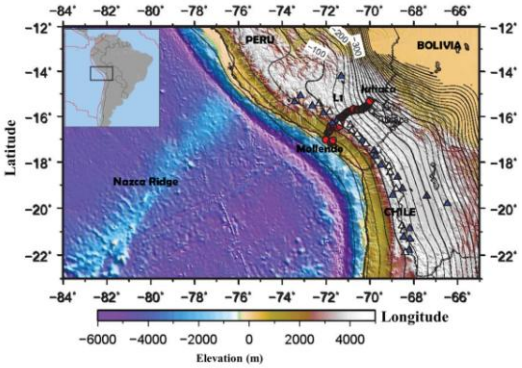

Figure 1. Map showing topography and bathymetry of southern Peru, location of the subducting Nazca Ridge, the Altiplano of the central Andes, slab contours of the Nazca plate based on fits to seismicity, the locations of seismic stations installed in Peru shown as red circles, and active and dormant volcanoes of the volcanic arc denoted by blue and white triangles respectively.

Data and Methods

The analysis in this paper is based on over two years of data (June, 2008 to August, 2010) recorded on the array shown in Figure 1. The receiver functions utilize phases from teleseismic earthquake with distance-magnitude windows designed to produce satisfactory signal to noise with minimal interference by other phases. The phases and their windows are: P-waves (>5.8 Mw, 30-90 degrees), PP-waves (>6.0 Mw, 90-180 degrees) and PKP waves (>6.4 Mw, 143-180 degrees). In total there were 69 P-phases, 69 PP-phases, and 48 PKP-phase events incorporated in this study. PKP phases were used because of the prevalence of events occurring in areas such as Indonesia, which are almost antipodal to Peru. Due to the almost vertical arrival angle of these phases, no conversion is expected at horizontal interfaces such as the Moho, however PKP phases can be used to detect dipping interfaces such as the slab. Individual records were bandpassed from .01 to 1 Hz. Receiver functions are constructed by the standard method described in Langston, 1979 and Yan and Clayton (2007). Source complexities and mantle propagation effects are minimized by deconvolving the radial component with the vertical. Frequency-domain deconvolution (Langston, 1979; Ammon et al., 1990) was used, with a water level cutoff and Gaussian filter applied for stability. RFs are stacked using the method of Zhu and Kanamori (2000) which uses the converted phase and multiples to obtain estimates of the depth of an interface and average Vp/Vs ratio above the interface. A search is done over a range of depths and Vp/Vs ratios based on stacks of many events from similar back-azimuths. A simple migrated image is then constructed by backprojecting the receiver functions along their ray paths. The angle from the station is estimated using the ray parameter and event backazimuth, with corrections for the station elevation. A simple layered velocity model was used to provide an approximation for conversion from receiver function time to depth.

Results

An image based on teleseismic P and PP receiver functions produced from data recorded by the seismic array with events from all azimuths is shown in Figure 2 (top). The Moho has an initial depth of around 25 km near the coast and steepens to around 75 km depth beneath the Altiplano. Also evident is a positive impedance mid-crustal signal at around 40 km depth. The subducting slab can be clearly observed in Figure 2 (bottom), which is a stack of data from the northwest azimuth. From the teleseismic (P) and PP phase receiver function results, a double pulse slab signal (negative overlying a positive signal) is observed most strongly down to a depth of around 100 kilometers depth which may be indicative of the transport of hydrous minerals in oceanic crust into the subduction zone (Kawakatsu et al, 2007). The transition between the positive and negative pulse is consistent with the location of the subducting Nazca plate as described by seismicity in the Wadati-Benioff zone.

Discussion

Our receiver function results for the normal subducting region of southern Peru show a Moho that deepens from 25 km near the coast to a depth of around 75 km beneath the Altiplano. Previous estimates of crustal thickness of the Altiplano are about 70-75 km (Cunningham and Roeker, 1986; Beck et al., 1996; Zandt et al, 1994). McGlashan et al. 2008 also estimated thicknesses from 59 to 70 in Southern Peru. The 75 km crust of the Altiplano is approximately the thickness required for the region to be in Airy isostatic equilibrium. A thick crust

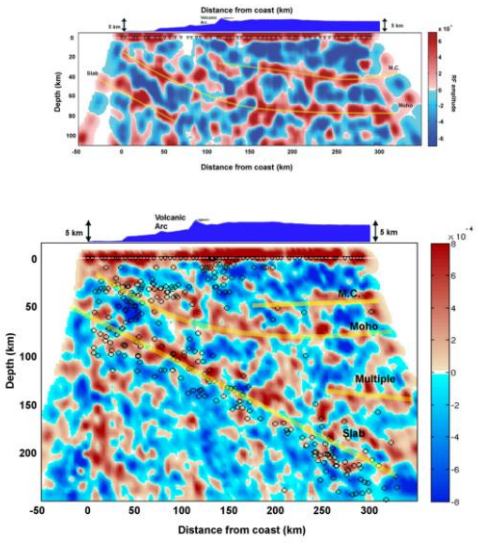

Figure 2: Top: Receiver function image of upper 120 km based on P and PP wave RFs showing Moho, mid-crustal structure, and part of subducting slab based on data from all azimuths. Bottom: Receiver function image showing full 250km, subducting slab, Moho picks from stacking, based on only data from the NW azimuth.

could be formed by shortening and several other processes.

The positive impedance structure observable at a depth of around 40 km is an unusual crustal feature because the crust does not formally have an interface with a sharp increase in velocity. One hypothesis that could explain this feature is under-thrusting by the Brazilian Craton. It is well accepted that this underthrusting exists as far as the Eastern Cordillera (McQuarrie et al., 2005; Gubbels et al., 1993; Lamb & Hoke, 1997; Beck & Zandt 02). However the results presented here appear to support the idea that it extends further to the west, as was suggested by Lamb and Hoke (1997).

The thickness of the crust under the Altiplano is related to the question of the timing of the rise of the Andes. The rapid rise model of Garzione et al (2008), proposes a gradual rise of 2 km over approximately 30 Myrs, followed by a rapid rise of 2 km over the last 10 Myrs. This is then used as evidence of lithospheric delamination because it is a process that can occur quickly. An alternative model of the rise suggests that all of it proceeded gradually over 40 Myrs. This latter model is favored by the mid-crustal layer found in this study. The presence of a deep crust to mantle transition as seen in the receiver functions suggests that the crust has doubled in thickness and the delamination of lower crust due to transition to eclogite with replacement by hot low density asthenosphere has not occurred.

Several authors (Allmendinger et al., 1997; Babeyko and Sobolev, 2005) suggest that there has been north-south variation in mechanisms and rates of crustal thickening and uplift in the central Andes; evolution in the Altiplano may have been different from what happened in the Puna plateau. A possible explanation for differential uplift in the Andes according to Babeyko and Sobolov (2005) comes from modeling which suggests that the mode of shortening is controlled by the strength of the foreland uppermost crust and temperature of the foreland lithosphere. So weak crust and cool lithosphere in the Altiplano could be supportive of underthrusting, shear shortening, and gradual uplift while further south in the Puna the strong sediments and warm lithosphere supports pure shear shortening, lithospheric delamination and resultant rapid uplift.

In addition to crustal information, receiver functions also show the subducting Nazca plate dipping at an angle of about 30 degrees from both the P/PP and PKP phases for Line 1. A figure showing a cartoon interpretation of the array data can be seen in Figure 3.

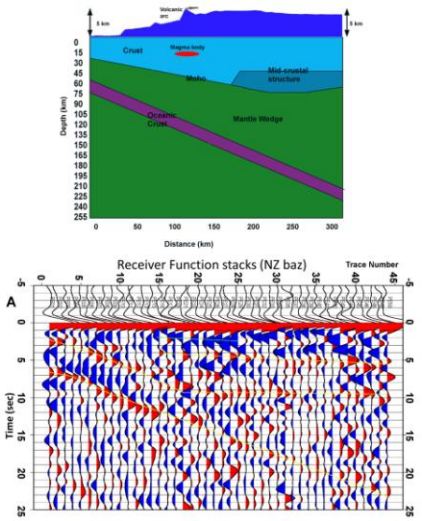

Figure 3: Top: Schematic model of receiver function images on left with the darker blue representing the underthrusting Brazilian shield, light blue representing the upper crust, purple representing the subducting oceanic crust, and magenta representing mantle. The small area of red represents a possible low velocity zone at around 20 km depth which may correspond to magmatism. Bottom: Sample receiver function traces based on data from the NW with lines tracing the major features shown in the top figure. The larger amplitude negative impedance pulses near the center may represent the magma body.

Conclusions

Receiver function studies using data from an array of 50 broadband stations in Southern Peru image the region of normal subduction beneath the Altiplano. The Moho is observed to have a maximum depth of 75 km beneath the Altiplano. The normally dipping slab is also clearly seen in the images. A positive impedance mid-crustal structure at about 40 km depth is seen in the receiver functions indicating an increase in velocity in the lower crust. This feature may be due to underthrusting of the Brazilian shield, previously believed to underlie the Eastern Cordillera but not extend beneath the entire Altiplano.

References

Allmendinger, R., and T. Gubbels (1996), Pure and simple shear plateau uplift, Altiplano-Puna, Argentina and Bolivia, Tectonophysics, 259, 1–13.

Allmendinger, R., T. Jordan, S. Kay, and B. Isacks (1997), The Evolution of the Altiplano-Puna Plateau of the Central Andes, Annu. Rev. Earth Planet. Sci., 25, 139–174.

Ammon, C., G. Randall, and G. Zandt (1990), On the nonuniqueness of receiver function inversions, J. Geophys. Res., 95 (B10), 15,303–15,318.

Babeyko, A., and S. Sobolev (2005), Quantifying different modes of the late Cenozoic shortening in the central Andes, Geology, 33 (8), 621–624.

Barnes, J., and T. Ehlers (2009), End member models for Andean Plateau uplift, Earth-Science Rev., 97 (105-132).

Beck, S., and G. Zandt (2002), The nature of orogenic crust in the Central Andes, J. of Geophys. Res., 107, 2230.

Beck, S., G. Zandt, S. Myers, T. Wallace, P. Silver, and L. Drake (1996), Crustal-thickness variations in the central Andes, Geology, 24 (5), 407–410.

Cunningham, P., and S. Roecker (1986), Three-dimensional P and S Wave Velocity Structures of Southern Peru and Their Tectonic Implications, Journal of Geophysical Research, 91 (B9), 9517–9532.

Ehlers, T., and C. Poulsen (2009), Influence of Andean uplift on climate and paleoaltimetry estimates, Earth and Planetary Science Letters, 281, 238–248.

Elger, K., O. Oncken, and J. Glodny (2005), Plateau-style accumulation of deformation: Southern Altiplano, Tectonics, 24 (TC4020).

Garzione, C., P. Molnar, J. Libarkin, and B. MacFadden (2006), Rapid late Miocene rise of the Bolivian Altiplano: Evidence for removal of mantle lithosphere, Earth and Planetary Science Letters, 241, 543–556.

Garzione, C., G. Hoke, J. Libarkin, S. Withers, B. MacFadden, J. Eiler, P. Ghosh, and A. Mulch (2008), Rise of the Andes, Science, 320, 1304–1307.

Ghosh, P., C. Garzione, and J. Eiler (2006), Rapid Uplift of the Altiplano Revealed Through 13C-18O Bonds in Paleosol Carbonates, Science, 311, 511–515.

Gregory-Wodzicki, K. (2000), Uplift history of the Central and Northern Andes; a review, Geol. Soc. Amer. Bull., 112 (7), 1091–1105.

Gubbels, T., B. Isacks, and E. Farrar (1993), High-level surfaces, plateau uplift, and foreland development, Bolivian central Andes, Geology, 21, 695–698.

Gutscher, M., W. Spakman, H. Bijwaard, and E. Engdahl (2000b), Geodynamics of flat subduction: Seismicity and tomographic constraints from the Andean margin, Tectonics, 19 (5), 814–833.

Hampel, A. (2002), The migration history of the Nazca Ridge along the Peruvian active margin: a re-evaluation, Earth and Planetary Science Letters, 203, 665–679.

Horton, B., B. Hampton, and G. Waanders (2001), Paleogene synorogenic sedimentation in the Altiplano Plateau and implications for initial mountain building in the Central Andes, Geol. Soc. Amer. Bull., 113, 1387–1400.

Kawakatsu, H., and S. Watada (2007), Seismic Evidence for Deep-Water Transportation in the Mantle, Science, 316, 1468-1471.

Lamb, S., and L. Hoke (1997), Origin of the high plateau in the Central Andes, Bolivia, South America, Tectonics, 16 (4), 623–649.

Langston, C. (1979), Structure under Mount Rainier, Washington, inferred from teleseismic body waves, J. Geophys. Res., 84, 4749–4762.

McGlashan, M., L. Brown, and S. Kay (2008), Crustal thickness in the Central Andes from teleseismically recorded depth phase precursors, Geophys. J. Int., 175, 1013-1022.

McQuarrie, N., B. Horton, G. Zandt, S. Beck, and P. DeCelles (2005), Lithospheric evolution of the Andean fold-thrust belt, Bolivia, and the origin of the central Andean plateau, Tectonophysics, 399, 15–37.

Oncken, O., J. Kley, K. Elger, P. Victor, and K. Schemmann (2006), Deformation of the Central Andean Upper Plate System - Facts, Fiction, and Constraints for Plateau Models, Springer, Berlin, p. 569.

Zandt, G., A. Velasco, and S. Beck (1994), Composition and thickness of the southern Altiplano crust, Bolivia, Geology, 22, 1003–1006.

Zhu, L., and H. Kanamori (2000), Moho depth variation in southern California from teleseismic receiver functions, J. Geophys. Res., 105 (B2), 2969–2980.